Mineralogical Magazine (2019), **83**, 349–360
doi:10.1180/mgm.2018.118

CAMBRIDGE UNIVERSITY PRESS

Article

Magnesioleydetite and straβmannite, two new uranyl sulfate minerals with sheet structures from Red Canyon, Utah

Anthony R. Kampf[1]*, Jakub Plášil[2], Anatoly V. Kasatkin[3], Barbara P. Nash[4] and Joe Marty[5]

[1]Mineral Sciences Department, Natural History Museum of Los Angeles County, 900 Exposition Boulevard, Los Angeles, CA 90007, USA; [2]Institute of Physics ASCR, v.v.i., Na Slovance 1999/2, 18221 Prague 8, Czech Republic; [3]Fersman Mineralogical Museum of the Russian Academy of Sciences, Leninsky Prospekt, 18-2, 119071, Moscow, Russia; [4]Department of Geology and Geophysics, University of Utah, Salt Lake City, Utah 84112, USA; and [5]5199 East Silver Oak Road, Salt Lake City, UT 84108, USA

Abstract

Magnesioleydetite (IMA2017-063), $Mg(UO_2)(SO_4)_2{\cdot}11H_2O$, and straβmannite (IMA2017-086), $Al(UO_2)(SO_4)_2F{\cdot}16H_2O$, are two new minerals from mines in Red Canyon, San Juan County, Utah, USA. Magnesioleydetite occurs in the Markey mine and straβmannite occurs in both the Markey and Green Lizard mines. Both minerals are secondary phases found in efflorescent crusts on the surfaces of mine walls. Magnesioleydetite occurs in irregular aggregates (to ~0.5 mm) of blades (to ~0.2 mm) exhibiting the following properties: transparent to translucent; pale green–yellow colour; vitreous lustre; white streak; non-fluorescent; brittle; Mohs hardness ≈ 2; irregular fracture; one perfect cleavage on {001}; and calculated density = 2.463 g/cm^3. Straβmannite occurs in irregular aggregates (to ~0.5 mm) of equant crystals (to ~0.2 mm) exhibiting the following properties: transparent; light yellow–green colour; vitreous to greasy lustre; nearly white streak; bright greenish-blue fluorescence; somewhat brittle, Mohs hardness ≈ 1½; irregular fracture; one good cleavage on {001}; measured and calculated densities of 2.20(2) and 2.173 g/cm^3, respectively; optically biaxial (–); $\alpha = 1.477(2)$, $\beta = 1.485(2)$ and $\gamma = 1.489(2)$ (white light); $2V_{meas.} = 72(2)°$; dispersion $r > v$ (slight); orientation $Y = \mathbf{b}$, $X \wedge \mathbf{c} = 20°$ (in obtuse β); pleochroism with X = nearly colourless, Y = pale green–yellow and Z = light green–yellow ($X < Y < Z$). The empirical formulas for magnesioleydetite and straβmannite are $(Mg_{0.56}Fe_{0.26}Zn_{0.11}Mn_{0.01})_{\Sigma 0.94}(U_{0.99}O_2)(S_{1.015}O_4)_2{\cdot}11H_2O$ and $Al_{1.00}Na_{0.16}(U_{0.99}O_2)(S_{1.00}O_4)_2[F_{0.58}(OH)_{0.42}]{\cdot}16H_2O$, respectively. Magnesioleydetite is monoclinic, $C2/c$, $a = 11.3513(3)$, $b = 7.7310(2)$, $c = 21.7957(15)$ Å, $\beta = 102.387(7)°$, $V = 1868.19(16)$ Å^3 and $Z = 4$. Straβmannite is monoclinic, $C2/c$, $a = 11.0187(5)$, $b = 8.3284(3)$, $c = 26.6727(19)$ Å, $\beta = 97.426(7)°$, $V = 2427.2(2)$ and $Z = 4$. The structures of magnesioleydetite ($R_1 = 0.016$ for 2040 $I > 2\sigma I$ reflections) and straβmannite ($R_1 = 0.0343$ for 2220 $I > 2\sigma I$ reflections) each contain uranyl-sulfate sheets based on the protasite-anion topology.

Keywords: magnesioleydetite, straβmannite, new mineral, uranyl sulfate, crystal structure, protasite-anion topology, Markey mine, Green Lizard mine, Utah, USA

(Received 22 December 2017; accepted 19 February 2018; Accepted Manuscript online: 28 May 2018; Associate Editor: Sergey Krivovichev)

Introduction

Several mines in Red Canyon in southeast Utah, USA, have in recent years yielded a remarkable array of new uranyl minerals. Of particular note are uranyl sulfates possessing a variety of structural motifs. Described herein are the new minerals magnesioleydetite and straβmannite, which possess topologically identical uranyl-sulfate sheets that are very similar to the uranyl-sulfate sheet in wetherillite, $Na_2Mg(UO_2)_2(SO_4)_4{\cdot}18H_2O$ (Kampf *et al.*, 2015*a*), another mineral described recently from this area.

Magnesioleydetite is named as the Mg analogue of leydetite, $Fe^{2+}(UO_2)(SO_4)_2{\cdot}11H_2O$ (Plášil *et al.*, 2013), with Mg replacing Fe^{2+} in the interlayer octahedral cation site. Straβmannite is named for German chemist Friedrich Wilhelm (Fritz) Straβmann (1902–1980) who worked with Otto Hahn and Lise Meitner on the discovery of nuclear fission (of uranium) in 1938. It was Straβmann who, in 1938, identified barium as a product of the bombardment of uranium with neutrons, direct evidence of the process of nuclear fission. Hahn received the Nobel Prize for Chemistry in 1944 for the discovery of nuclear fission. Straβmann served as Director of the Max Planck Institute for Chemistry from 1949 to 1953 and later founded the Institute of Nuclear Chemistry. In 1966, U.S. President Lyndon Johnson presented the Enrico Fermi Award to Hahn, Meitner and Straβmann. He and his wife were recognised in 1985 by the Yad Vashem Institute (Jerusalem) as "Righteous Among the Nations" for hiding a Jew in their home in Germany during World War II. In 1989, the International Astronomical Union named an asteroid for him, 19136 Straβmann.

The new minerals and their names were approved by the Commission on New Minerals, Nomenclature and Classification of the International Mineralogical Association based upon proposals IMA2017-063 for magnesioleydetite and IMA2017-086 for straβmannite. All type specimens have been deposited in the collections of the Natural History Museum of Los Angeles County,

*Author for correspondence: Anthony R. Kampf, Email: akampf@nhm.org
Cite this article: Kampf A.R., Plášil J., Kasatkin A.V., Nash B.P. and Marty J. (2019) Magnesioleydetite and straβmannite, two new uranyl sulfate minerals with sheet structures from Red Canyon, Utah. *Mineralogical Magazine* **83**, 349–360. https://doi.org/10.1180/mgm.2018.118

900 Exposition Boulevard, Los Angeles, CA 90007, USA. The four magnesioleydetite cotypes have been assigned catalogue numbers 66647, 66648, 66649 and 66650; however, the magnesioleydetite crystals originally on all of these specimens have largely transformed to a lower hydrate, although remnant domains of magnesioleydetite may remain in some crystals. There are also four straβmannite cotypes, two each from the Green Lizard (67264 and 67265) and Markey (67266 and 67267) mines.

Occurrence

Magnesioleydetite was found underground in the Markey mine (37°32′57″N, 110°18′08″W). Straβmannite was first discovered on specimens collected underground in the Green Lizard mine (37°34′37.10″N, 110°17′52.80″W) and was later found underground in the Markey mine. Both mines are in the White Canyon mining district, San Juan County, Utah, USA, ~72 km west of the town of Blanding, Utah. The Green Lizard mine is near the head of Low Canyon on the east side of Red Canyon, 2.1 km north of the Blue Lizard mine. The Green Lizard mine is also a type locality for greenlizardite (Kampf *et al.*, 2018*b*), shumwayite (Kampf *et al.*, 2017*b*) and meitnerite (Kampf *et al.*, 2018*c*). The Markey mine is also a type locality for feynmanite (Kampf *et al.*, 2019), leószilárdite (Olds *et al.*, 2017) and markeyite (Kampf et al., 2018*a*).

The Markey mine is ~1 km southwest of the Blue Lizard mine, on the west side of Red Canyon. The geology of both mines (see below) is similar to that of the Blue Lizard mine (Kampf *et al.*, 2017*a*; Chenoweth, 1993). Mineralised channels are in the Shinarump member of the Chinle Formation. The Shinarump member consists of medium- to coarse-grained sandstone, conglomeratic sandstone beds and thick siltstone lenses. Ore minerals were deposited as replacements of wood and other organic material and as disseminations in the enclosing sandstone. Since the mines closed, oxidation of primary ores in the humid underground environment has produced a variety of secondary minerals, mainly sulfates, as efflorescent crusts on the surfaces of mine walls.

Magnesioleydetite and straβmannite are both rare minerals. At the Markey mine, they are found together on asphaltum in association with arsenuranospathite, gypsum, metakahlerite, nováčekite-II, uramarsite and at least one additional potentially new Mg uranyl sulfate. At the Green Lizard mine, straβmannite is found on matrix comprised of mainly subhedral to euhedral, equant quartz crystals that are recrystallised counterparts of the original grains of the sandstone; some asphaltum is intermixed with the quartz grains. It is associated with gypsum, halotrichite, rozenite and the Mg analogue of rietveldite.

The principal factors that are likely to control the formation of the various uranyl-sulfate phases at the Blue Lizard mine were discussed by Kampf *et al.* (2017*a*) and these also apply, to similar mines in the area, including the Green Lizard and Markey mines. Briefly, these minerals form at ambient temperature by evaporative processes at the surface of a rock with high relative porosity. The environment is relatively oxidising (high Eh) and solutions are generally acidic (low pH). The relative acidity prevalent during the formation of any given phase can be interpreted from its crystal structure (and, specifically, its structural unit) by considering the charge deficiency per anion (CDA) calculated using the bond-valence approach (*cf.* Hawthorne and Schindler, 2008; Hawthorne, 2012); higher CDA correlates with higher pH. The molar proportions of S and U in the formulas of the various uranyl sulfates are indicative of the relative concentrations of these elements in solution during formation. Minerals with higher molar proportions of U relative to S can be inferred to form closer to the source of U and, therefore, probably earlier in the paragenesis. The molar proportion of H_2O can be expected to decrease with decreasing relative humidity as evaporative processes proceed during formation.

The uranyl-sulfate sheet structural units in magnesioleydetite and straβmannite, being topologically identical, yield a CDA of 0.22 valence units (vu) for both minerals, as well as for wetherillite, which has a similar uranyl-sulfate sheet. Therefore, we can expect all three minerals to form at about the same pH – intermediate among the new uranyl-sulfate phases listed by Kampf *et al.* (2017*a*), which range in CDA from 0.10 vu (shumwayite) to 0.34 vu (belakovskiite). Magnesioleydetite and straβmannite have the same proportion of U relative to S (U:S = 1:2). By comparison, among the new uranyl sulfates from the area, shumwayite and plášilite have the highest proportions of U *vs.* S (U:S = 1:1), while belakovskiite has the lowest (U:S = 1:5). Therefore, both magnesioleydetite and straβmannite can be expected to form relatively near the source of the U. Finally, it is notable that straβmannite has a much greater molar proportion of H_2O than magnesioleydetite, suggesting that it formed later than straβmannite during progressive evaporation from the porous rock surface.

Besides straβmannite, the only other phases with essential F that have been confirmed from the uranium mines in Red Canyon are uranospathite, $Al(UO_2)_2(PO_4)_2F{\cdot}20H_2O$, and arsenuranospathite, $Al(UO_2)_2(AsO_4)_2F{\cdot}20H_2O$, both of which are also secondary phases and are found at the Markey mine. The well-known affinity of Al for F explains why essential Al and F are both found in all three of these phases. It may be that there were Al fluoride complexes in the solutions from which these minerals formed; however, it is clear that F is quite rare in these deposits and no precursor F-bearing phases have been identified.

Physical and optical properties

Magnesioleydetite

Magnesioleydetite occurs as transparent to translucent, pale green–yellow blades up to ~0.2 mm long, commonly growing in irregular aggregates to ~0.5 mm across (Fig. 1). Blades are flattened on {001}; no other forms could be measured, but the general crystal shape can be generated with the additional forms $\{11\bar{1}\}$ and $\{10\bar{1}\}$, combined with twinning by 180° rotation on $[1\bar{1}0]$ (indicated by single-crystal X-ray diffraction); the composition plane appears to be $\{11\bar{1}\}$ (Fig. 2). The lustre is vitreous, the streak is white and the mineral is non-fluorescent. Crystals are somewhat brittle, with Mohs hardness of ~2, irregular fracture and one perfect cleavage on {001}. The density could not be measured because of the scarcity and small size of crystals. The calculated density is 2.463 g/cm^3 for the empirical formula and 2.434 g/cm^3 for the ideal formula. Small crystal size, small amount of material, crystal twinning and the tendency of crystals to dehydrate all conspired to make the determination of optical properties impossible. The optical properties of leydetite could only be determined partially for some of the same reasons. It is likely that magnesioleydetite has indices of refraction similar to those of leydetite: $\alpha' = 1.513$ and $\gamma' = 1.522$. The average index of refraction predicted by the Gladstone–Dale relationship is

https://doi.org/10.1180/mgm.2018.118 Published online by Cambridge University Press

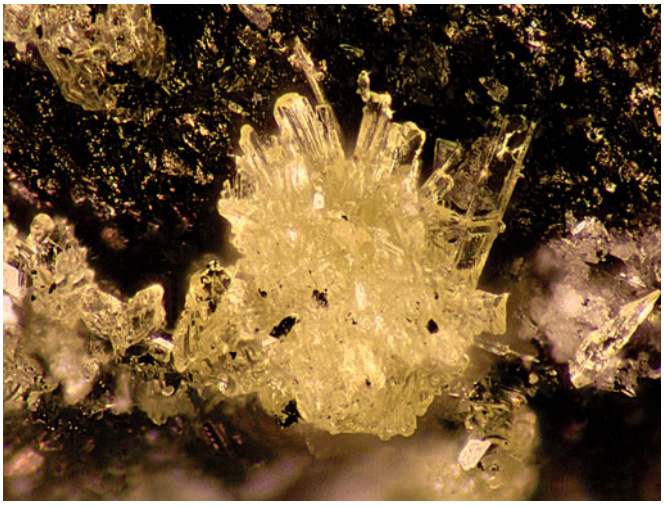

Fig. 1. Magnesioleydetite. The field of view is 1.5 mm across.

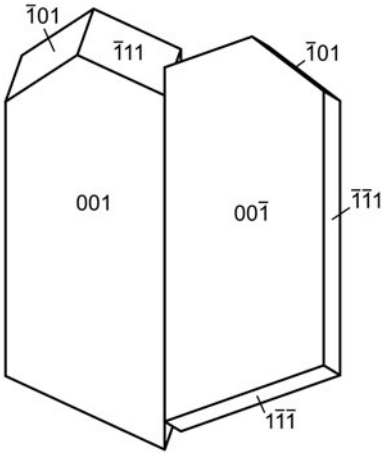

Fig. 2. Crystal drawing of magnesioleydetite twin, clinographic projection in non-standard orientation, [1$\bar{1}$0] vertical.

1.512 for magnesioleydetite. The mineral is easily soluble in room-temperature H_2O and dehydrates readily even at moderate relative humidity. The crystal used for the structure determination transformed to a lower hydrate following data collection, despite being coated with Apiezon grease.

Straβmannite

Light yellow–green, equant, transparent straβmannite crystals to 0.2 mm occur in irregular aggregates to ~0.5 mm across (Fig. 3). It has nearly white streak and exhibits bright greenish-blue fluorescence in 405 nm light. It is somewhat brittle, with Mohs hardness of ~1½, irregular fracture and one good cleavage on {001}. The density measured by flotation in a mixture of methylene iodide and toluene is 2.20(2) g/cm^3. The calculated densities are 2.173 g/cm^3 for the empirical formula and 2.179 g/cm^3 for the ideal formula. Straβmannite is optically biaxial (–) with $\alpha = 1.477(2)$, $\beta = 1.485(2)$ and $\gamma = 1.489(2)$ (white light). The 2V measured directly on a spindle stage is 72(2)°; the calculated 2V is 70.2°. There is slight $r > v$ dispersion. The optical orientation is $Y = \mathbf{b}$ and $X \wedge \mathbf{c} = 20°$ in the obtuse

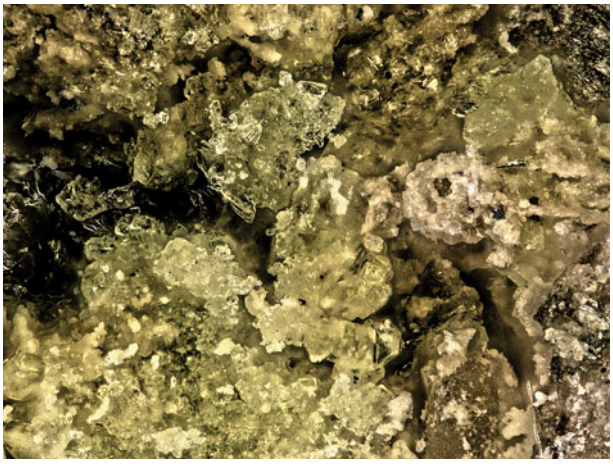

Fig. 3. Indistinct intergrowths of straβmannite crystals (pale yellow) with rozenite (white) on quartz/asphaltum matrix from the Green Lizard mine. The field of view is 0.84 mm across.

angle β and the pleochroism is X = nearly colourless, Y = pale green–yellow, Z = light green–yellow; and $X < Y < Z$. Straβmannite is easily soluble in room-temperature H_2O.

Raman spectroscopy

Raman spectroscopy was conducted on a Horiba XploRA PLUS. The spectrum for magnesioleydetite was recorded from 4000 to 100 cm^{-1} using a 532 nm diode laser. Straβmannite exhibited pronounced fluorescence using a 532 nm diode laser; consequently, its spectrum was recorded from 2000 to 100 cm^{-1} using a 785 nm diode laser. The spectrum for magnesioleydetite was featureless between 2800 and 1600 cm^{-1}, and that for straβmannite was featureless between 2000 and 1200 cm^{-1}. The spectra from 1800 to 100 cm^{-1} for both minerals are compared in Fig. 4 and the spectrum for magnesioleydetite in the 4000 to 2500 cm^{-1} region is shown as a vertically exaggerated insert in Fig. 4.

Magnesioleydetite

A broad band composed of several overlapping bands between ~3600 cm^{-1} and 3200 cm^{-1} is attributed to the ν O–H stretching vibrations of the H_2O molecules. According to the empirical correlation given by Libowitzky (1999) the H···A lengths of the corresponding hydrogen bonds are in the range of 2.4 to 1.8 Å. The weak feature at ~2932 cm^{-1} is most probably due to organic impurities. A very weak, broad band at 1593 cm^{-1} is connected with the ν_2 (δ) H–O–H bending vibration of the H_2O molecules. The low intensity of the ν_2 (δ) H_2O vibration is not uncommon in Raman, as the technique is sensitive to a change of the tensor of polarisability, and not for a dipole moment.

Weak bands with shoulders around 1200–1100 cm^{-1} [1203 (sh), 1190, 1125 and 1083 cm^{-1}] are attributed to split triply degenerate ν_3 antisymmetric stretching vibration of the SO_4 tetrahedra. Compared to them, the bands related to the ν_1 symmetric stretching vibrations of SO_4 tetrahedra have higher intensities: 1049 and 1032 cm^{-1} (with shoulders at 1027 and 1010 cm^{-1}). The number of split bands is in line with the presence of two symmetrically non-equivalent SO_4 tetrahedra in the structure (*cf.* bluelizardite or synthetic klaprothite; Plášil *et al.*, 2016). The

https://doi.org/10.1180/mgm.2018.118 Published online by Cambridge University Press

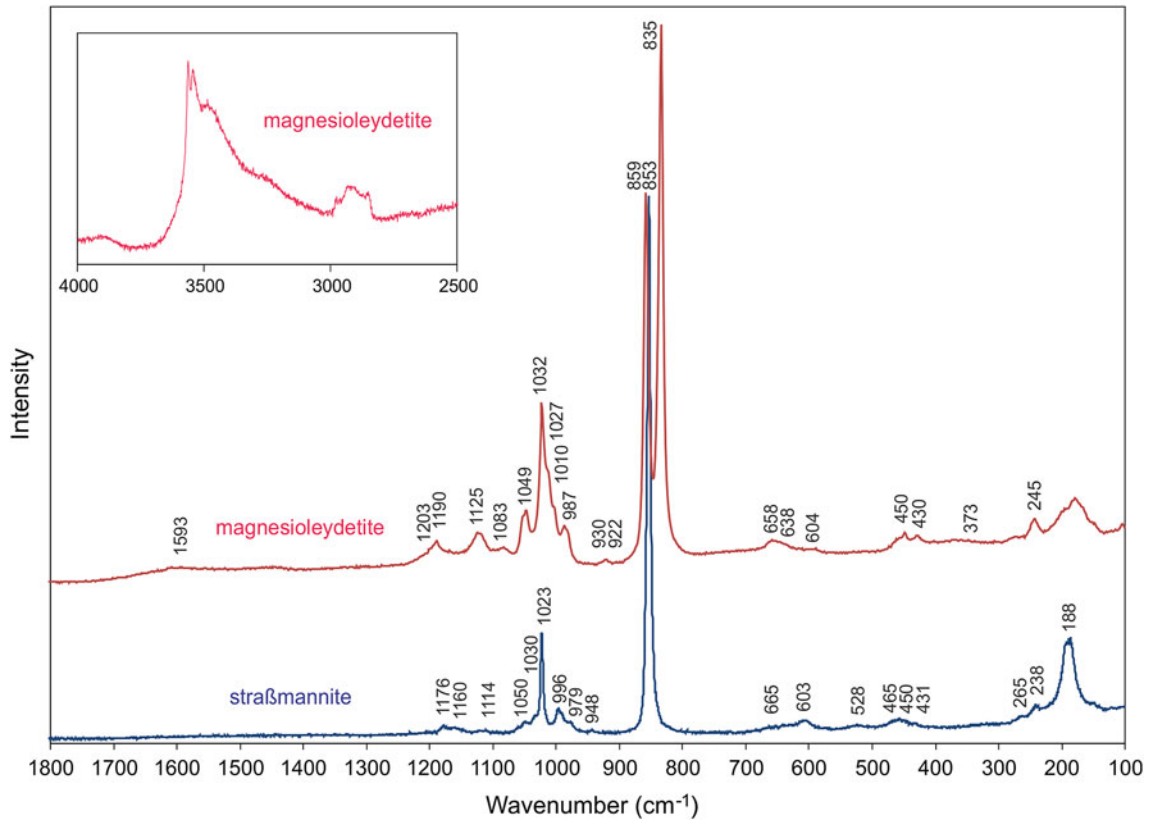

Fig. 4. Raman spectra of magnesioleydetite (532 nm laser) and straβmannite (785 nm laser). Note that the insert showing the magnesioleydetite spectrum from 4000 to 2500 cm^{-1} is vertically exaggerated (×10) relative to the spectrum from 1300 to 100 cm^{-1}. See text for band assignments.

weak band at 987 cm^{-1} may be attributed to δ U–O–H vibration. A weak, two-component band at 930 and 922 cm^{-1} is assigned to the ν_3 antisymmetric stretching vibration of the uranyl ion, UO_2^{2+}; and the two-component, very strong, partially overlapping bands at 859 and 835 cm^{-1} are assigned to the ν_1 symmetric U–O stretching vibration of UO_2^{2+}. In the crystal structure, there is only one unique U atom, so the two peaks cannot represent splitting due to symmetrically independent U atoms. Therefore, we conclude that one of these peaks is an artifact, probably caused by some organic matter (C–C stretches; compare e.g. Quilès and Burneau, 1998; Unruh *et al.*, 2013; Kampf *et al.*, 2015*b*) as a surface contaminant. This is well supported also by the presence of C–H bands at ~2900 cm^{-1}. Note that the crystal had been preserved in Apiezon grease, which was removed with xylene prior to the recording of the Raman spectrum. Based on inferred U–O bond lengths (after Bartlett and Cooney, 1989) for UO_2^{2+} of ~1.78 and ~1.75 Å (ν_1 835 and 859 cm^{-1}), we conclude that the band at 835 cm^{-1} is attributable to ν_1 UO_2^{2+}. The bond lengths inferred from the wavenumber of ν_3 UO_2^{2+} are ~1.76 and ~1.77 Å.

Weak Raman bands at 658, 638 and 604 cm^{-1} are attributed to the ν_4 (δ) triply degenerate antisymmetric stretching vibrations of SO_4 tetrahedra. Weak Raman bands 450 and 430 cm^{-1} are related to the split ν_2 (δ) doubly degenerate bending vibrations of SO_4.

The band at 373 cm^{-1} can be attributed to Mg–O stretching vibrations (*cf.* Kampf *et al.*, 2015*a*,*c*; Plášil *et al.*, 2010, 2016; Volkovich *et al.*, 1998). A strong Raman band at 245 cm^{-1}, with shoulders at to both higher and lower energies are most probably overlapping ν_2 (δ) doubly degenerate bending vibration

Table 1. Chemical composition (in wt.%) for magnesioleydetite.

Constituent	Mean	Range	S.D.	Probe standard
MgO	3.24	2.42–3.95	0.63	syn. MgF_2
MnO	0.06	0–0.28	0.06	syn. $MnTa_2O_6$
FeO	2.69	2.07–4.15	0.65	syn. Fe_2O_3
ZnO	1.33	0.94–2.19	0.44	syn. ZnO
SO_3	23.32	21.20–26.12	1.79	syn. FeS_2
UO_3	40.69	38.22–43.15	1.73	syn. UO_2
H_2O*	28.80			
Total	100.13			

*Based on the structure.
S.D. – standard deviation.

Table 2. Chemical composition (in wt.%) for straβmannite.

Constituent	Mean	Range	S.D.	Probe standard
Na_2O	0.64	0.46–0.90	0.17	albite
Al_2O_3	6.41	4.49–8.09	1.52	sanidine
UO_3	35.74	32.04–40.23	3.00	syn. UO_2
SO_3	20.28	16.88–22.59	2.17	baryte
F	1.40	0.84–1.95	0.33	syn. CaF_2
H_2O*	36.27			
O = F	−0.59			
Total*	100.15			

*Based on the structure.
S.D. – standard deviation.

https://doi.org/10.1180/mgm.2018.118 Published online by Cambridge University Press

Table 3. Powder X-ray diffraction data (d in Å) for magnesioleydetite. Only calculated lines with $I \geq 2$ are listed.

I_{obs}	I_{calc}	d_{obs}	d_{calc}	*hkl*
100	**100**	**10.66**	**10.6442**	**0 0 2**
78	**36**	**6.31**	**6.2925**	**$\bar{1}$ 1 1**
38	23, 8	5.85	5.8833, 5.7680	1 1 1, $\bar{1}$1 1 2
14	12	5.57	5.5435	2 0 0
49	**47**	**5.32**	**5.3221**	**0 0 4**
15	21	5.17	5.1759	1 1 2
61	**34**	**5.06**	**5.0461**	**$\bar{1}$ 1 3**
19	5, 12	4.502	4.5343, 4.4642	2 0 2, 1 1 3
17	9	4.323	4.3313	$\bar{2}$ 0 4
9	4, 2	3.885	3.8655, 3.8506	0 2 0, 1 1 4
36	24	3.759	3.7545	$\bar{1}$ 1 5
16	16,	3.628	3.6333,	0 2 2,
	4		3.5481	0 0 6
17	14	3.466	3.4839	2 0 4
59	**25**	**3.390**	**3.3962,**	**$\bar{3}$ 1 1**
	2		3.3735	$\bar{3}$ 1 2
	3		3.3498	1 1 5
23	14	3.268	3.2713	$\bar{3}$ 1 3
50	**17, 9, 6**	**3.193**	**3.2008, 3.1938, 3.1708**	**3 1 1, $\bar{2}$ 2 1, 2 2 0**
23	14,3	3.138	3.1463, 3.1276	$\bar{2}$ 2 2, 0 2 4
21	10, 7	3.045	3.0816, 3.0370	2 2 1, $\bar{2}$ 2 3
	3		2.9462	1 1 6
	2		2.9130	$\bar{3}$ 1 5
16	14	2.885	2.8836	$\bar{1}$ 1 7
25	8, 4	2.824	2.8347, 2.8153	$\bar{4}$ 0 2, 3 1 3
6	4,	2.773	2.7710,	2 2 3,
	3		2.7339	2 0 6
18	9, 2	2.701	2.7071, 2.7050	$\bar{2}$ 2 5, $\bar{3}$ 1 6
	4		2.6610	0 0 8
5	2, 2	2.622	2.6197, 2.6139	1 1 7, 0 2 6
11	2, 5, 2	2.582	2.6076, 2.5879, 2.5521	3 1 4, 2 2 4, 4 0 2
	2		2.5231	$\bar{2}$ 2 6
12	4, 2	2.506	2.5101, 2.5008	1 3 0, $\bar{3}$ 1 7
18	7, 3, 4	2.475	2.4789, 2.4700, 2.4546	1 3 1, $\bar{1}$ 3 2, $\bar{4}$ 0 6
6	2, 2, 3	2.411	2.4170, 2.4086, 2.4034	1 3 2, 3 1 5, $\bar{1}$ 3 3
9	3, 3, 3	2.319	2.3311, 2.3140, 2.3110	1 3 3, $\bar{1}$ 3 4, $\bar{1}$ 1 9
5	3, 2	2.274	2.2859, 2.2525	$\bar{4}$ 2 2, 4 2 0
14	4, 2	2.220	2.2203, 2.2178	2 0 8, $\bar{4}$ 2 4
	2		2.2098	$\bar{1}$ 3 5
	2		2.2002	4 2 1
21	5, 5	2.163	2.1683, 2.1657	$\bar{5}$ 1 3, $\bar{4}$ 0 8
	2		2.1475	$\bar{2}$ 0.10
29	4, 7, 2, 4	2.120	2.1322, 2.1298, 2.1178, 2.1138	1 1 9, 4 2 2, 1 3 5, 3 3 0
	3		2.0975	$\bar{3}$ 3 3
	2		2.0859	$\bar{5}$ 1 5
38	4, 8, 2, 6	2.0684	2.0788, 2.0721, 2.0574, 2.0529	5 1 1, $\bar{4}$ 2 6, 3 1 7, $\bar{3}$ 3 4
7	2, 2, 2	2.0086	2.0183, 2.0038, 1.9837	$\bar{2}$ 2 9, 1 3 6, $\bar{1}$ 3 7
	2		1.9344	5 1 3
9	3, 3	1.9235	1.9248, 1.9179	0 4 1, $\bar{1}$ 1.11
22	2, 2, 2, 3	1.8815	1.8913, 1.8902, 1.8867, 1.8772,	1 3 7, $\bar{6}$ 0 2, 3 3 4, $\bar{2}$ 2.10
12	3, 3, 2	1.8537	1.8647, 1.8614, 1.8478	0 2.10, 4 2 5, 6 0 0
	2		1.8294	$\bar{2}$ 4 1
14	3, 3, 2, 3	1.8037	1.8075, 1.8058, 1.7984, 1.7907	2 4 1, $\bar{2}$ 0 12, $\bar{2}$ 4 3, 1 1.11
	3		1.7832	1 3 8
27	2, 3, 2, 2, 3, 3	1.7683	1.7760, 1.7740, 1.7674, 1.7658, 1.7650, 1.7639	$\bar{5}$ 1 9, 3 1 9, 4 2 6, 5 1 5, $\bar{2}$ 4 4, $\bar{3}$ 3 8
	2		1.7420	4 0 8
	2		1.7381	2 4 3
27	2, 8	1.6960	1.7024, 1.6981	$\bar{4}$ 2.10, $\bar{6}$ 2 2
17	2, 3,2	1.6781	1.6833, 1.6808, 1.6651	$\bar{5}$ 3 4, 5 3 0, $\bar{4}$ 0.12
7	3	1.6309	1.6356	$\bar{6}$ 2 6
17	2, 2, 2, 3	1.5956	1.6072, 1.6014, 1.6004, 1.5975	$\bar{5}$ 1.11, $\bar{3}$ 3.10, 6 2 2, 5 1 7
9	2, 2	1.5614	1.5677, 1.5643	$\bar{7}$ 1 5, 3 3 8

The strongest lines are given in bold

https://doi.org/10.1180/mgm.2018.118 Published online by Cambridge University Press

Table 4. Powder X-ray diffraction data (*d* in Å) for straβmannite. Only calculated lines with $I \geq 2$ are listed.

I_{obs}	I_{calc}	d_{obs}	d_{calc}	*hkl*
100	**100**	**13.24**	**13.2140**	**0 0 2**
53	**13, 43**	**6.61**	**6.6181, 6.6070**	**1 1 0, 0 0 4**
26	**30**	**6.11**	**6.1117**	**$\bar{1}$ 1 2**
35	**38**	**5.74**	**5.7406**	**1 1 2**
	2		5.5017	$\bar{1}$ 1 3
7	6	5.46	5.4591	2 0 0
4	4	4.861	4.8699	$\bar{1}$ 1 4
22	22	4.494	4.5032	1 1 4
8	10	4.377	4.4047	0 0 6
	2		4.2970	$\bar{1}$ 1 5
7	7	4.155	4.1606	0 2 0
	2		4.1099	0 2 1
8	8	3.968	3.9649	2 0 4
11	13	3.806	3.8065	$\bar{1}$ 1 6
2	4	3.660	3.6667	$\bar{2}$ 0 6
19	17, 5	3.535	3.5414, 3.5207	1 1 6, 0 2 4
	3		3.3955	$\bar{1}$ 1 7
	2		3.3578	$\bar{3}$ 1 1
38	**7,13,21**	**3.324**	**3.3344, 3.3276, 3.3091**	**3 1 0, $\bar{3}$ 1 2, 2 2 0**
	2		3.3035	0 0 8
20	9, 6	3.265	3.2707, 3.2523	$\bar{2}$ 2 2, 2 2 1
23	**6, 7, 10**	**3.138**	**3.1524, 3.1461, 3.1291**	**2 2 2, 3 1 2, $\bar{3}$ 1 4**
	2		3.0559	$\bar{2}$ 2 4
11	3, 8	3.016	3.0246, 3.0029	0 2 6, $\bar{2}$ 0 8
	2		2.9088	$\bar{2}$ 2 5
7	6	2.863	2.8676,	1 1 8
	2		2.8448	3 1 4
	2		2.8239	$\bar{3}$ 1 6
	3		2.7509	$\bar{2}$ 2 6
	2		2.7441	$\bar{4}$ 0 2
8	5	2.731	2.7295	4 0 0
	2		2.6883	1 3 0
11	8	2.656	2.6508	$\bar{1}$ 3 2
	3		2.6428	0 0 10
6	3	2.618	2.6182	1 3 2
	2		2.6074	4 0 2
10	3, 7	2.519	2.5232, 2.5181	$\bar{1}$ 1 10, $\bar{1}$ 3 4
3	2, 2	2.453	2.4629, 2.4349	1 3 4, $\bar{2}$ 2 8
5	2, 2, 2	2.402	2.4153, 2.3974, 2.3909	4 0 4, 2 2 7, 1 1 10
2	3	2.323	2.3278	$\bar{1}$ 3 6
	2		2.2630	1 3 6
3	2, 2	2.233	2.2327, 2.2308	$\bar{4}$ 2 4, 0 2 10
13	2, 3, 5	2.204	2.2094, 2.2060, 2.2023	4 2 2, 3 3 0, 0 0 12
11	4, 2, 4	2.141	2.1488, 2.1434, 2.1404	3 3 2, $\bar{3}$ 3 4 , $\bar{2}$ 0 12
	2		2.1274	$\bar{5}$ 1 2
8	3, 2, 2	2.115	2.1219, 2.1183, 2.1121	$\bar{4}$ 2 6, $\bar{1}$ 3 8, 5 1 0
9	7, 2	2.0845	2.0888, 2.0803	$\bar{5}$ 1 4, 0 4 0
10	2, 3, 2	2.0451	2.0550, 2.0463, 2.0424	0 4 2, 5 1 2, 1 1 12
8	2, 2, 2	1.9833	1.9906, 1.9825, 1.9802	2 2 10, 4 0 8, $\bar{4}$ 2 8
8	3	1.9440	1.9439	2 4 0
7	2, 2, 2	1.9104	1.9153, 1.9135, 1.9106	$\bar{1}$ 3 10, 3 3 6, 2 4 2
	2		1.9033	$\bar{2}$ 2 12
3	2	1.8859	1.8885	$\bar{2}$ 4 4
5	2, 2	1.8438	1.8539, 1.8421	$\bar{1}$ 1 14, 2 4 4
7	2	1.8173	1.8182	5 1 6
4	2, 2	1.7773	1.7718, 1.7707	3 3 8, 2 2 12
7	3	1.7601	1.7604	$\bar{5}$ 1 10
8	2, 3	1.7257	1.7328, 1.7239	$\bar{3}$ 1 14, $\bar{5}$ 3 2
5	2	1.7038	1.7031	$\bar{5}$ 3 4
6	2, 2	1.6766	1.6777, 1.6672	$\bar{4}$ 2 12, 6 2 0

The strongest lines are given in bold

of the UO_2^{2+} and U–O_{eq}–*ligand* stretching modes (*cf.* Bullock and Parret, 1970; Ohwada, 1976; Brittain *et al.*, 1985; Plášil *et al.*, 2010). Weak bands at the lowest energies can be assigned to unclassified lattice modes, most probably skeletal vibrations of the entire sheet of polyhedra.

Straβmannite

Bands at 1176, 1160 and 1114 cm^{-1} are attributed to the split triply degenerate ν_3 antisymmetric stretching vibration of the SO_4 tetrahedra. A band at 1050 cm^{-1} could be also related to the stretching vibrations of the SO_4 tetrahedra; however, there is only one symmetrically unique S site in the structure of straβmannite, so the assignment is of this band is disputable. A narrow band at 1023 cm^{-1} with a shoulder at 1030 cm^{-1} is assigned to the ν_1 symmetric stretching vibrations of the SO_4 tetrahedra. The assignment of the bands of weak intensity at 996 and 979 cm^{-1} is not clear. A very weak band at 948 cm^{-1} may be related to the ν_3 antisymmetric stretching vibration of the uranyl ion, UO_2^{2+}. A very strong band at 853 cm^{-1} is assigned to the ν_1 symmetric U–O stretching vibration of the UO_2^{2+} ion. The inferred U–O bond lengths (after Bartlett and Cooney, 1989) in the uranyl ion of ~1.76 Å (from ν_1) are in line with those derived from the X-ray study (see below). Weak Raman bands at 665 and 603 cm^{-1} are attributed to the ν_4 (δ) triply degenerated antisymmetric stretching vibrations of the SO_4 tetrahedra. Weak Raman bands at 528, 465, 450 and 431 (sh) cm^{-1} are related to the split ν_2 (δ) doubly degenerate bending vibrations of the SO_4. Bands at 265 and 238 cm^{-1} are most probably related to the ν_2 (δ) doubly degenerate bending vibration of the UO_2^{2+}. A quite intense band at 188 cm^{-1} is most probably a lattice mode.

Chemical composition

Magnesioleydetite

Electron probe microanalyses (EPMA) were performed (on 8 points) in the laboratory of the Fersman Mineralogical Museum using a CamScan 4D electron microprobe in energy-dispersive spectroscopy mode (20 kV, 5 nA and 3 μm beam diameter). Attempts to use wavelength-dispersive spectroscopy with a higher beam current were made, but resulted in partial dehydration of the mineral and significantly higher totals. H_2O was not determined directly because of extreme paucity of material. The H_2O content was calculated by stoichiometry on the basis of 3 U + S and 21 O apfu as indicated by the crystal-structure refinement. The Raman spectrum confirms the presence of H_2O and the absence of B–O, C–O and N–O bonds in the mineral. Analytical data are given in Table 1.

The empirical formula based on the criteria above is $(Mg_{0.56}Fe_{0.26}Zn_{0.11}Mn_{0.01})_{\Sigma 0.94}(U_{0.98}O_2)(S_{1.01}O_4)_2{\cdot}11H_{2.01}O$. The ideal formula is $Mg(UO_2)(SO_4)_2{\cdot}11H_2O$ which requires MgO 5.89, SO_3 23.39, UO_3 41.78 and H_2O 28.95, total 100 wt.%. The Gladstone–Dale compatibility index could not be computed because the indices of refraction could not be determined.

Straβmannite

Electron probe microanalyses (5 points on two crystals from the Green Lizard mine and 3 points on one crystal from the Markey mine) were performed at the University of Utah on a Cameca SX-50 electron microprobe with four wavelength-dispersive spectrometers and using *Probe for EPMA* software. Analytical conditions were: accelerating voltage = 15 keV, beam current = 10 nA and a beam diameter = 10 μm. Raw X-ray intensities were corrected for matrix effects with a φρ(z) algorithm (Pouchou and Pichoir, 1991). Time-dependent intensity corrections were applied to Al, U, S and F; no systematic variation in Na was noted during analyses. Straβmannite was very challenging

https://doi.org/10.1180/mgm.2018.118 Published online by Cambridge University Press

Table 5. Data collection and structure-refinement details for magnesioleydetite and straβmannite.

	Magnesioleydetite	Straβmannite
Crystal data		
Structural formula	$(Mg_{0.56}Fe_{0.26}Zn_{0.18})(UO_2)(SO_4)_2{\cdot}11H_2O$	$Al(UO_2)(SO_4)_2F(H_2O)_{16}$
Crystal dimensions (μm)	160 × 70 × 40	70 × 60 × 30
Crystal system, space group	Monoclinic, *C*2/*c*	Monoclinic, *C*2/*c*
Temperature (K)	293(2)	293(2)
a, *b*, *c* (Å)	11.3513(3), 7310(2), 21.7957(15)	11.0187(5), 8.3284(3), 26.6727(19)
β (°)	102.387(7)	97.426(7)
V (Å^3)	1868.19(16)	2427.2(2)
Z	4	4
Density (g/cm^3)	2.490	2.179
Absorption coefficient (mm^{-1})	9.445	7.006
Data collection		
Instrument	Rigaku R-Axis Rapid II	Rigaku R-Axis Rapid II
Radiation type, wavelength (Å)	Mo*K*α, λ = 0.71075	Mo*K*α, λ = 0.71075
X-ray power	50 kV, 40 mA	50 kV, 40 mA
F(000)	1331.5	1544
θ range	3.53 to 27.48°	3.08 to 27.46°
Absorption correction	Multi-scan (ABSCOR, Higashi, 2001)	Multi-scan (ABSCOR, Higashi, 2001)
Reflections measured, independent	8487, 2110	19124, 2739
Reflections with $I > 2\sigma I$	2040	2220
R_{int}	0.026	0.073
Index ranges	$-14 \le h \le 14$	$-14 \le h \le 14$
	$-10 \le k \le 10$	$-9 \le k \le 10$
	$-27 \le l \le 28$	$-34 \le l \le 34$
Refinement		
Data completeness to θ max (%)	98.9	98.9
Refinement method	Full-matrix least-squares on F^2	Full-matrix least-squares on F^2
Parameter/restraints	149/11	201/30
GoF	1.114	1.061
Final *R* indices [$I > 2\sigma I$]	$R_1 = 0.0161$, $wR_2 = 0.0348$	$R_1 = 0.0343$, $wR_2 = 0.0667$
R indices (all data)	$R_1 = 0.0169$, $wR_2 = 0.0350$	$R_1 = 0.0456$, $wR_2 = 0.0724$
$\Delta\rho_{max}$, $\Delta\rho_{min}$ (e^- A^{-3})	+0.91/−0.67	+1.52/−1.29

$R_{int} = \Sigma|F_o^2 - F_o^2(\text{mean})|/\Sigma[F_o^2]$. GoF = $S = \{\Sigma[w(F_o^2-F_c^2)^2]/(n-p)\}^{1/2}$. $R_1 = \Sigma||F_o|-|F_c||/\Sigma|F_o|$. $wR_2 = \{\Sigma[w(F_o^2-F_c^2)^2]/\Sigma[w(F_o^2)^2]\}^{1/2}$; $w = 1/[\sigma^2(F_o^2)+(aP)^2+bP]$ and P is $[2F_c^2+\text{Max}(F_o^2,0)]/3$; for magnesioleydetite a is 0.0154 and b is 1.9286; for straβmannite a is 0.0243 and b is 12.6098.

Table 6. Atom coordinates and displacement parameters (Å^2) for magnesioleydetite.

	x/*a*	*y*/*b*	*z*/*c*	U_{eq}	Occ.	U^{11}	U^{22}	U^{33}	U^{23}	U^{13}	U^{12}
U	0	0.20592(2)	¼	0.01424(5)	1	0.01144(7)	0.01318(7)	0.01856(7)	0	0.00424(4)	0
S	0.30824(6)	0.36607(8)	0.28936(3)	0.01860(13)	1	0.0173(3)	0.0155(3)	0.0245(3)	−0.0011(2)	0.0079(2)	−0.0020(3)
Mg*	0	½	0	0.02634(17)	$Mg_{0.56}Fe_{0.26}Zn_{0.18}$	0.0335(4)	0.0236(4)	0.0221(4)	0.0006(3)	0.0064(3)	0.0021(3)
O1	0.2857(2)	0.4801(3)	0.33826(10)	0.0334(5)	1	0.0417(13)	0.0282(11)	0.0340(12)	−0.0084(9)	0.0162(9)	−0.0008(10)
O2	0.3775(2)	0.2150(3)	0.31627(10)	0.0331(5)	1	0.0396(13)	0.0275(11)	0.0343(12)	0.0088(9)	0.0129(10)	0.0120(10)
O3	0.19402(18)	0.3113(3)	0.24741(10)	0.0282(4)	1	0.0200(10)	0.0286(11)	0.0377(12)	−0.0060(9)	0.0097(8)	−0.0067(9)
O4	0.37668(17)	0.4576(2)	0.24769(9)	0.0230(4)	1	0.0197(9)	0.0212(9)	0.0306(10)	−0.0008(8)	0.0107(8)	−0.0075(8)
O5	0.03506(18)	0.2037(3)	0.33310(9)	0.0268(4)	1	0.0249(10)	0.0309(11)	0.0247(10)	−0.0038(8)	0.0053(8)	−0.0037(9)
OW6	0.000000	0.5167(4)	0.250000	0.0413(9)	1	0.041(2)	0.0154(15)	0.078(3)	0	0.0371(18)	0
H6	−0.036(3)	0.583(4)	0.2668(18)	0.050	1						
OW7	0.0764(3)	0.7268(3)	0.47353(12)	0.0399(6)	1	0.0575(16)	0.0323(12)	0.0343(13)	−0.0031(10)	0.0193(12)	−0.0136(12)
H7a	0.100(4)	0.808(4)	0.4981(17)	0.048	1						
H7b	0.098(4)	0.736(5)	0.4408(15)	0.048	1						
OW8	0.1094(2)	0.3485(3)	0.45511(11)	0.0385(5)	1	0.0408(13)	0.0481(14)	0.0273(11)	−0.0116(10)	0.0089(10)	−0.0015(12)
H8a	0.084(4)	0.312(5)	0.4197(13)	0.046	1						
H8b	0.181(2)	0.378(5)	0.4583(18)	0.046	1						
OW9	0.3673(2)	0.0139(3)	0.41863(11)	0.0419(6)	1	0.0510(16)	0.0432(15)	0.0265(12)	0.0080(10)	−0.0024(10)	−0.0159(12)
H9a	0.379(4)	0.074(5)	0.3920(16)	0.050	1						
H9b	0.320(3)	−0.055(5)	0.4058(18)	0.050	1						
OW10	0.1823(2)	0.7789(3)	0.37316(11)	0.0356(5)	1	0.0463(15)	0.0341(13)	0.0263(12)	0.0002(10)	0.0073(10)	0.0069(11)
H10a	0.208(4)	0.705(4)	0.3576(18)	0.043	1						
H10b	0.151(3)	0.836(5)	0.3443(15)	0.043	1						
OW11	0.3430(3)	0.4680(3)	0.46503(12)	0.0436(6)	1	0.0535(16)	0.0365(13)	0.0375(13)	−0.0005(12)	0.0023(12)	0.0087(12)
H11a	0.345(4)	0.473(6)	0.4310(13)	0.052	1						
H11b	0.371(4)	0.383(4)	0.4820(18)	0.052	1						

https://doi.org/10.1180/mgm.2018.118 Published online by Cambridge University Press

Table 7. Atom coordinates and displacement parameters (Å^2) for straβmannite.

	x/a	*y/b*	*z/c*	U_{eq}	Occ.	U^{11}	U^{22}	U^{33}	U^{23}	U^{13}	U^{12}
U	½	−0.00640(3)	¼	0.02151(9)	1	0.01681(14)	0.02298(16)	0.02484(14)	0	0.00302(9)	0
Al	½	½	½	0.0279(5)	1	0.0285(11)	0.0301(13)	0.0247(10)	−0.0002(9)	0.0022(8)	−0.0011(10)
S	0.21223(11)	0.15901(15)	0.28046(5)	0.0245(3)	1	0.0188(6)	0.0222(7)	0.0325(7)	−0.0004(5)	0.0030(5)	0.0006(5)
O1	0.2754(4)	0.2476(5)	0.32301(14)	0.0362(9)	1	0.037(2)	0.036(2)	0.034(2)	−0.0040(17)	0.0012(16)	−0.0068(18)
O2	0.1450(4)	0.0225(4)	0.29843(15)	0.0379(9)	1	0.036(2)	0.032(2)	0.047(2)	0.0054(17)	0.0075(17)	−0.0082(18)
O3	0.1267(3)	0.2639(5)	0.24835(13)	0.0330(9)	1	0.025(2)	0.033(2)	0.041(2)	0.0015(16)	0.0028(16)	0.0099(16)
O4	0.2999(3)	0.0974(5)	0.24697(14)	0.0331(9)	1	0.0204(19)	0.037(2)	0.042(2)	−0.0073(17)	0.0058(15)	0.0043(16)
O5	0.5191(3)	−0.0072(4)	0.31642(13)	0.0307(8)	1	0.0282(19)	0.037(2)	0.0270(18)	−0.0005(15)	0.0042(14)	−0.0024(17)
F/OW1	0.5462(4)	0.2904(5)	0.49825(14)	0.0428(9)	0.5 F / 0.5 O	0.046(2)	0.044(2)	0.039(2)	0.0001(17)	0.0067(17)	0.0027(19)
H1A	0.542(12)	0.223(10)	0.520(3)	0.051	0.5						
H1B	0.582(11)	0.248(12)	0.477(3)	0.051	0.5						
OW2	0.3439(4)	0.4437(5)	0.46821(15)	0.0374(9)	1	0.035(2)	0.035(2)	0.041(2)	−0.0035(19)	−0.0029(17)	−0.0025(19)
H2A	0.293(5)	0.509(5)	0.457(2)	0.045	1						
H2B	0.327(5)	0.358(4)	0.459(2)	0.045	1						
OW3	0.5548(4)	0.5322(6)	0.43668(14)	0.0423(10)	1	0.036(2)	0.063(3)	0.027(2)	−0.001(2)	0.0026(17)	−0.012(2)
H3A	0.619(4)	0.573(8)	0.433(2)	0.051	1						
H3B	0.513(5)	0.520(7)	0.4099(15)	0.051	1						
OW4	½	0.2897(7)	¼	0.0422(14)	1	0.029(3)	0.027(3)	0.068(4)	0	−0.003(3)	0
H4A	0.438(4)	0.343(7)	0.239(2)	0.051	1						
OW5	0.6569(4)	0.1248(6)	0.42960(16)	0.0455(11)	1	0.043(3)	0.048(3)	0.047(3)	0.002(2)	0.011(2)	0.005(2)
H5A	0.603(10)	0.060(13)	0.421(3)	0.055	0.5						
H5B	0.673(6)	0.169(7)	0.4044(16)	0.055	1						
H5C	0.628(12)	0.195(9)	0.446(3)	0.055	0.5						
OW6	0.7739(5)	0.2809(6)	0.35911(16)	0.0508(12)	1	0.062(3)	0.049(3)	0.041(3)	−0.003(2)	0.007(2)	0.004(2)
H6A	0.735(6)	0.335(7)	0.3375(19)	0.061	1						
H6B	0.806(6)	0.211(6)	0.344(2)	0.061	1						
OW7	0.4495(5)	−0.0715(6)	0.42719(16)	0.0520(12)	1	0.065(3)	0.048(3)	0.041(3)	0.008(2)	0.000(2)	−0.008(2)
H7A	0.511(7)	−0.030(16)	0.419(4)	0.062	0.5						
H7B	0.412(6)	−0.112(8)	0.4025(17)	0.062	1						
H7C	0.445(12)	−0.132(11)	0.451(2)	0.062	0.5						
OW8	0.2724(4)	0.1678(5)	0.42221(15)	0.0419(10)	1	0.045(3)	0.042(3)	0.038(2)	0.0011(19)	0.0032(19)	−0.003(2)
H8A	0.264(5)	0.198(7)	0.3930(13)	0.050	1						
H8B	0.325(5)	0.100(7)	0.426(2)	0.050	1						
OW9	0.4284(4)	0.5120(5)	0.34688(15)	0.0407(10)	1	0.040(2)	0.050(3)	0.032(2)	−0.0066(19)	0.0073(17)	−0.012(2)
H9A	0.482(4)	0.517(7)	0.329(2)	0.049	1						
H9B	0.388(5)	0.433(6)	0.338(2)	0.049	1						

to analyse. It was impossible to obtain a good polish and crystal surfaces suffered further because of crystal dehydration. The wide ranges in analytical values are probably largely the result of the poor crystal surfaces. Because insufficient material is available for a direct determination of H_2O, it is calculated by stoichiometry on the basis of 3 U + S and 27 O + F + Na apfu as indicated by the structure determination. Note that Na is assumed to substitute for H_2O in the interlayer region in the structure. Analytical data are given in Table 2.

The empirical formula based upon the criteria above is $Al_{1.00}Na_{0.16}(U_{0.99}O_2)(S_{1.005}O_4)_2[F_{0.58}(OH)_{0.42}]\cdot 15.84H_{1.99}O$. The simplified formula is $Al(UO_2)(SO_4)_2F\cdot 16H_2O$, which requires Al_2O_3 6.40, UO_3 35.92, SO_3 20.11, F 2.39 and H_2O 36.19, O = F −1.00, total 100 wt.%. The Gladstone–Dale compatibility index (Mandarino, 2007), $1 - (K_P/K_C)$, for the empirical formula is −0.013 (superior) based on the empirical formula and −0.030 (excellent) based on the ideal formula, in both cases using $k(UO_3) = 0.118$, as provided by Mandarino (1976).

X-ray crystallography and structure refinement

Powder X-ray studies were carried out using a Rigaku R-Axis Rapid II curved imaging plate microdiffractometer, with monochromatised Mo$K\alpha$ radiation ($\lambda = 0.71075$ Å). A Gandolfi-like motion on the ϕ and ω axes was used to randomise the samples and observed *d* values and intensities were derived by profile fitting using *JADE 2010* software (Materials Data, Inc.). The powder data for magnesioleydetite (Table 3) and those for straβmannite (Table 4) show good agreement with the patterns calculated from the structure determinations.

Table 8. Selected bond distances (Å) and angles (°) for magnesioleydetite.

Mg–OW9 ×2	2.068(2)	U–O5 ×2	1.769(2)	S–O1	1.447(2)
Mg–OW7 ×2	2.091(2)	U–O3 ×2	2.360(2)	S–O2	1.459(2)
Mg–OW8 ×2	2.096(2)	U–O4 ×2	2.370(2)	S–O3	1.479(2)
<Mg–O>	2.085	U–OW6	2.403(3)	S–O4	1.494(2)
		<U1–O_{Ur}>	1.769	<S–O>	1.470
		<U1–O_{eq}>	2.373		

Hydrogen bonds *D*–H···*A*	*D*–H	H···*A*	*D*···*A*	<*DHA*
OW6–H6···O2 ×2	0.79(2)	1.91(2)	2.689(3)	171(4)
OW7–H7a···OW11	0.83(3)	1.96(3)	2.770(4)	165(4)
OW7–H7b···OW10	0.81(3)	1.95(3)	2.742(3)	168(4)
OW8–H7a···O5	0.81(3)	2.03(3)	2.842(3)	174(4)
OW8–H8b···OW11	0.84(3)	1.94(3)	2.772(4)	175(4)
OW9–H9a···O2	0.78(3)	1.98(3)	2.742(3)	170(4)
OW9–H9b···OW10	0.77(3)	2.03(3)	2.793(4)	174(4)
OW10–H10a···O1	0.75(2)	2.04(3)	2.771(3)	165(4)
OW10–H10b···O4	0.79(2)	2.18(3)	2.922(3)	159(4)
OW11–H11a···O1	0.75(3)	1.99(3)	2.701(3)	159(5)
OW11–H11b···OW8	0.79(3)	2.23(3)	2.984(4)	159(4)

https://doi.org/10.1180/mgm.2018.118 Published online by Cambridge University Press

Table 9. Selected bond distances (Å) and angles (°) for straβmannite.

U–O5 ×2	1.757(3)	Al–OW1 ×2	1.820(4)	S–O1	1.454(4)
U–O4 ×2	2.360(3)	Al–OW2 ×2	1.877(4)	S–O2	1.471(4)
U–O3 ×2	2.372(4)	Al–OW3 ×2	1.885(4)	S–O3	1.475(4)
U–OW4	2.466(6)	<Al–O>	1.861	S–O4	1.489(4)
<U1–O_{Ur}>	1.757			<S–O>	1.472
<U1–O_{eq}>	2.386				

Hydrogen bonds *D*–H···*A*	*D*–H	H···*A*	*D*···*A*	<*DHA*
OW1–H1A···OW7	0.81(3)	1.88(3)	2.694(6)	174(14)
OW1–H1B···OW5	0.81(3)	1.90(4)	2.706(6)	173(12)
OW2–H2A···OW5	0.80(3)	1.86(3)	2.651(6)	169(6)
OW2–H2B···OW8	0.77(3)	1.92(3)	2.675(6)	167(6)
OW3–H3A···OW8	0.80(3)	1.92(3)	2.722(6)	179(6)
OW3–H3B···OW9	0.80(3)	1.82(3)	2.616(6)	173(6)
OW4–H4A···O2	0.83(3)	1.96(4)	2.729(6)	153(6)
OW5–H5A···OW7	0.82(3)	2.04(5)	2.804(7)	156(11)
OW5–H5B···OW6	0.81(3)	1.98(3)	2.741(6)	158(7)
OW5–H5C···F	0.82(3)	1.92(4)	2.706(6)	159(9)
OW6–H6A···O2	0.81(3)	2.06(3)	2.845(6)	164(6)
OW6–H6B···OW9	0.81(3)	2.13(3)	2.857(7)	149(6)
OW7–H7A···OW5	0.81(3)	2.05(5)	2.804(7)	153(10)
OW7–H7B···OW6	0.80(3)	2.00(4)	2.765(7)	159(7)
OW7–H7C···F	0.81(3)	1.89(4)	2.694(6)	171(15)
OW8–H8A···O1	0.81(3)	1.93(3)	2.733(5)	168(6)
OW8–H8B···OW7	0.81(3)	1.98(3)	2.781(7)	174(6)
OW9–H9A···O2	0.81(3)	2.06(3)	2.858(6)	167(7)
OW9–H9B···O1	0.81(3)	1.99(3)	2.796(6)	173(6)

For both minerals, the single-crystal structure data were collected at room temperature using the same diffractometer and radiation noted above. The straβmannite crystal used was from the Green Lizard mine. The data were processed using the Rigaku *CrystalClear* software package and empirical (multi-scan) absorption corrections were applied using the *ABSCOR* program (Higashi, 2001) in the *CrystalClear* software suite. The structures were solved by direct methods using *SIR2011* (Burla *et al.*, 2012) and *SHELXL-2013* (Sheldrick, 2015) was used for the refinements of the structures. Difference-Fourier syntheses located all H atom positions for both structures, which were then refined with soft restraints of 0.82(3) Å on the O–H distances and 1.30(3) Å on the H–H distances, and with the U_{eq} of each H set to 1.2 times that of the donor O atom.

Table 10. Bond-valence analysis for magnesioleydetite. Values are expressed in valence units.*

				Hydrogen bonds		
	Mg	U	S	Accepted	Donated	Σ
O1			1.60	0.19, 0.23		2.02
O2			1.55	0.23, 0.21		1.99
O3		0.51 ×2↓	1.47			1.98
O4		0.50 ×2↓	1.42	0.15		2.07
O5		1.80 ×2↓		0.17		1.97
OW6		0.47			−0.23, −0.23	0.01
OW7	0.35 ×2↓				−0.21, −0.20	−0.06
OW8	0.35 ×2↓				−0.17, −0.19	−0.01
OW9	0.37 ×2↓				−0.21, −0.19	−0.03
OW10				0.21, 0.19	−0.19, −0.15	0.06
OW11				0.20, 0.19	−0.23, −0.13	0.03
Σ	2.14	6.09	6.04			

*Multiplicity is indicated by ×↓. The bond valences associated with the Mg site are based on the assigned occupancy for the site ($Mg_{0.56}Fe_{0.26}Zn_{0.18}$). Cation–O bond valence parameters are from Gagné and Hawthorne (2015). Hydrogen-bond strengths based on O–O bond lengths from Ferraris and Ivaldi (1988).

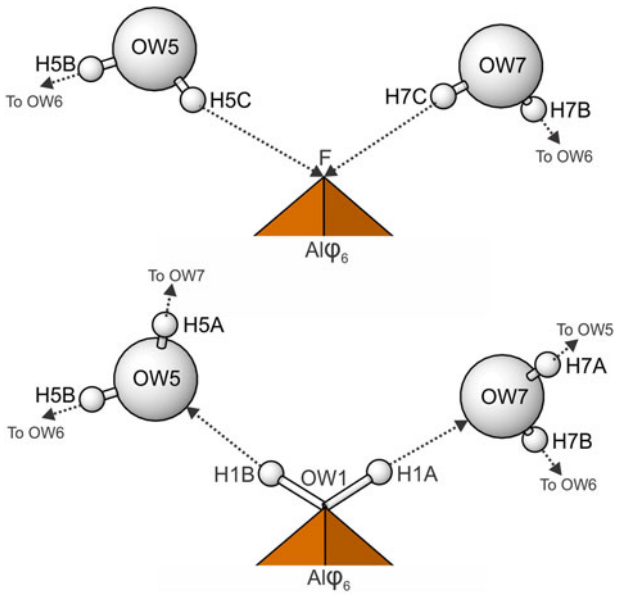

Fig. 5. Hydrogen bonding configurations for the F/OW1 site in the straβmannite structure depending upon whether the site is occupied by F (top) or O (bottom). Hydrogen bonds are shown with dashed lines.

Magnesioleydetite

The crystal used for the structure determination consisted of a single individual with a small twinned component; the omission of 20 reflections compensated for most of the overlap problems. The site-scattering value (mean atomic number × site

Table 11. Bond-valence analysis for straβmannite. Values are expressed in valence units.*

				Hydrogen bonds		
	Al	U	S	Accepted	Donated	Σ
O1			1.57	0.21, 0.19		1.97
O2			1.50	0.21, 0.17, 0.16		2.04
O3		0.50	1.49			1.99
O4		0.51	1.44			1.95
O5		1.84				1.84
F	0.48			0.22, 0.23		0.93
OW1	0.62				−0.23, −0.22	0.17
OW2	0.54 ×2↓				−0.25, −0.24	0.05
OW3	0.53 ×2↓				−0.22, −0.28	0.03
OW4		0.41			−0.21 ×2	−0.01
OW5				0.11, 0.25, 0.09	−0.09, −0.21, −0.11	0.04
OW6				0.21, 0.20	−0.17, −0.16	0.08
OW7				0.11, 0.09, 0.19	−0.09, −0.20, −0.11	−0.01
OW8				0.24, 0.22	−0.21, −0.19	0.06
OW9				0.28, 0.16	−0.16, −0.19	0.09
Σ	3.24	6.13	6.00			

*Multiplicity is indicated by ×↓. Al–O and U–O bond-valence parameters are from Gagné and Hawthorne (2015). Al–F bond-valence parameters are from Brown and Altermatt (1985). Hydrogen-bond strengths based on O–O bond lengths from Ferraris and Ivaldi (1988). Bond valences of ±0.09 and ±0.11 for OW5 and OW7 represent ½ hydrogen bonds accepted and donated.

https://doi.org/10.1180/mgm.2018.118 Published online by Cambridge University Press

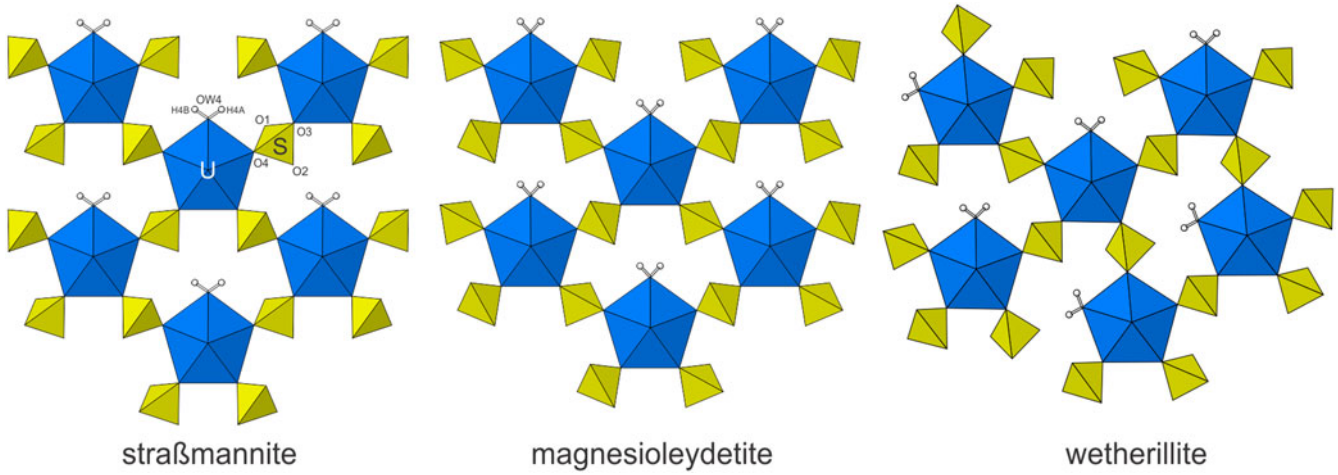

Fig. 6. The uranyl-sulfate sheets in straβmannite, magnesioleydetite and wetherillite. Note the different orientations of the SO_4 tetrahedra for straβmannite and magnesioleydetite, which define different geometrical isomers of topologically identical uranyl-sulfate sheets.

multiplicity) for the Mg site refined to 76.67 e^-. In the final refinement cycles, this site was assigned an occupancy of $Mg_{0.56}Fe_{0.26}Zn_{0.18}$, which corresponds to a site-scattering value of 75.52 e^-. Data collection and refinement details are given in Table 5, atom coordinates and displacement parameters in Table 6, selected bond distances in Table 8 and a bond valence analysis in Table 10.

Straβmannite

The Al–OW1 bond (1.813 Å) is very short for an Al–O bond, but quite reasonable for an Al–F bond. The average EPMA indicates only enough F to occupy ~29% of this site [corresponding to $F_{0.29}OH_{0.21}(H_2O)_{0.5}$ in the site and $F_{0.58}(OH)_{0.42}(H_2O)$ in the formula unit] and, considering the range in F content, the EPMA suggests that this site does not have more than ~50% occupancy by F. The difference-Fourier map provided no indication that the OW1 site is split into separate O and F sites and efforts to force splitting of this site were unsuccessful, probably owing to the fact that they would only need to be separated by ~0.05 Å to obtain optimal bond distances to Al. Ultimately, this site was refined with joint occupancy by O and F, providing an occupancy of 0.50(7) each for O and F. Note that the H atoms associated with OW1 were included in the O/F occupancy refinement for the OW1 site. The bond-valence analysis suggested that the H atoms associated with OW5 and OW7 have different configurations, depending on the occupancy of the OW1 site, such that when the OW1 site is occupied by F, it receives hydrogen bonds from OW5 and OW7, but when the OW1 site is an H_2O, it contributes hydrogen bonds to OW5 and OW7 (Fig. 5). Difference-Fourier revealed one fully occupied H site and two half-occupied H sites each for OW5 and OW7 in line with the hydrogen-bonding scheme supported by the bond-valence analysis. The structural placement of the small amount of Na indicated in the chemical analysis is not entirely clear; however, it seems quite likely that it replaces some of the H_2O in the interlayer region, and this has been taken into consideration for the basis of the empirical formula. Data collection and refinement details are given in Table 5, atom coordinates and displacement parameters in Table 7, selected bond distances in Table 9 and a bond-valence analysis in Table 11.

The crystallographic information files have been deposited with the Principal Editor of *Mineralogical Magazine* and are available as Supplementary material (see below).

Description and discussion of the structures

In both structures, the U sites are surrounded by seven O atoms forming squat UO_7 pentagonal bipyramids. This is the most typical coordination for U^{6+}, particularly in uranyl sulfates, where the two short apical bonds of the bipyramid constitute the UO_2 uranyl group. The UO_7 bipyramids share four of their equatorial vertices with SO_4 tetrahedra. Each SO_4 tetrahedron, in turn, shares two of its vertices with UO_7 bipyramids. The remaining unshared equatorial vertex of the bipyramid is occupied by an H_2O group, which forms hydrogen bonds to one of the free vertices of the SO_4 tetrahedron. The linkages of the UO_7 bipyramids and sulfate tetrahedra form a $[(UO_2)(SO_4)_2(H_2O)]$ sheet parallel to {001} that is based upon a derivative of the protasite anion topology, graph notation I1/2b (see Lussier *et al.*, 2016).

Magnesioleydetite is the same as that of leydetite, $Fe^{2+}(UO_2)(SO_4)_2{\cdot}11H_2O$ (Plášil *et al.*, 2013), with Mg replacing Fe^{2+} in the interlayer octahedral cation site. The synthetic equivalent of magnesioleydetite was reported by Serezhkin *et al.* (1981). The uranyl-sulfate sheets in the structures of magnesioleydetite and straβmannite are topologically identical, but are geometrical isomers. The sheets are similar to those in wetherillite, $Na_2Mg(UO_2)_2(SO_4)_4{\cdot}18H_2O$ (Kampf *et al.*, 2015*a*); however, the sheet in wetherillite is topologically distinct, in that alternate rows of bipyramids are rotated in orientation (Fig. 6).

Besides their topologically identical sheets, the structures of magnesioleydetite and straβmannite are also similar in that their interlayer regions contain octahedra and isolated H_2O groups that link the sheets to one another only through hydrogen bonding. The straβmannite interlayer region is significantly thicker and contains more than twice as much H_2O (Fig. 7).

Acknowledgements. Igor Pekov and an anonymous reviewer are thanked for their constructive comments on the manuscript. A portion of this study

https://doi.org/10.1180/mgm.2018.118 Published online by Cambridge University Press

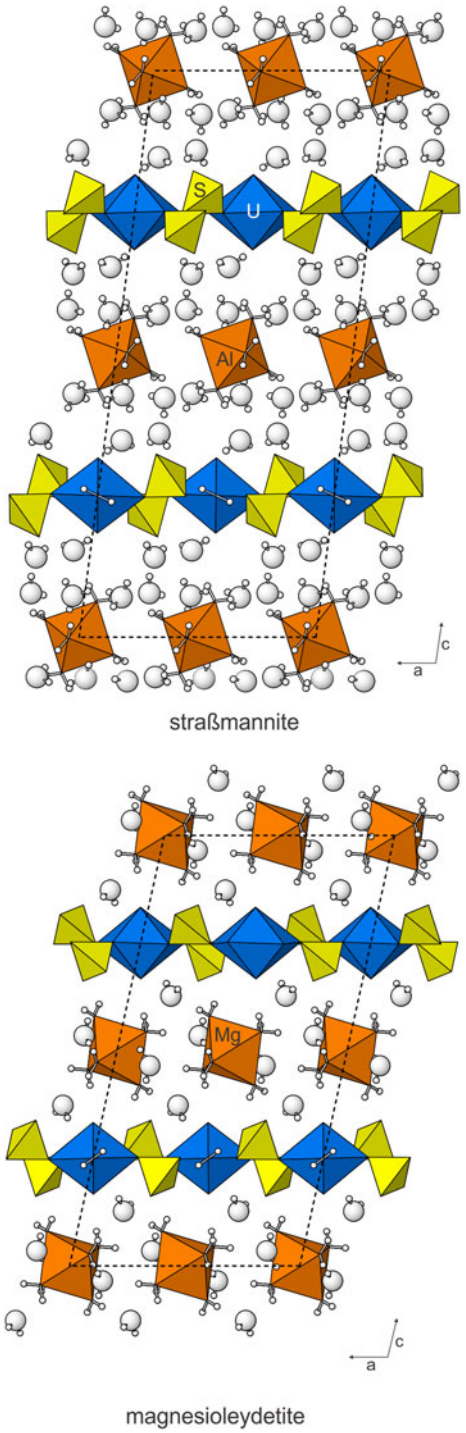

Fig. 7. The structures of straβmannite and magnesioleydetite viewed down [010]. The unit cells are shown by dashed lines.

was funded by the John Jago Trelawney Endowment to the Mineral Sciences Department of the Natural History Museum of Los Angeles County. JP acknowledges support of the Czech Science Foundation (project GACR 17-09161S).

Supplementary material. To view supplementary material for this article, please visit https://doi.org/10.1180/mgm.2018.118

References

Bartlett J.R. and Cooney R.P. (1989) On the determination of uranium-oxygen bond lengths in dioxouranium(VI) compounds by Raman spectroscopy. *Journal of Molecular Structure*, **193**, 295–300.

Brittain H.G., Ansari P., Toivonen J., Niinisto L., Tsao L. and Perry D.L. (1985) Photophysical studies of uranyl complexes. VIII. Luminiscence spectra of $UO_2SO_4{\cdot}3½H_2O$ and two polymorphs of bis(urea) uranyl sulfate. *Journal of Solid State Chemistry*, **59**, 259–264.

Brown I.D. and Altermatt D. (1985) Bond-valence parameters from a systematic analysis of the inorganic crystal structure database. *Acta Crystallographica*, **B41**, 244–247.

Bullock H. and Parret F.W. (1970) The low frequency infrared and Raman spectroscopic studies of some uranyl complexes: the deformation frequency of the uranyl ion. *Canadian Journal of Chemistry*, **48**, 3095–3097.

Burla M.C., Caliandro R., Camalli M., Carrozzini B., Cascarano G.L., Giacovazzo C., Mallamo M., Mazzone A., Polidori G. and Spagna R. (2012) *SIR*2011: a new package for crystal structure determination and refinement. *Journal of Applied Crystallography*, **45**, 357–361.

Chenoweth W.L. (1993) The geology and production history of the uranium deposits in the White Canyon mining district, San Juan County, Utah. *Utah Geological Survey Miscellaneous Publication*, 93–3.

Ferraris G. and Ivaldi G. (1988) Bond valence vs. bond length in O···O hydrogen bonds. *Acta Crystallographica*, **B44**, 341–344.

Gagné O.C. and Hawthorne F.C (2015) Comprehensive derivation of bond-valence parameters for ion pairs involving oxygen. *Acta Crystallographica*, **B71**, 562–578.

Hawthorne F.C. (2012) A bond-topological approach to theoretical mineralogy: crystal structure, chemical composition and chemical reactions. *Physics and Chemistry of Minerals*, **39**, 841–874.

Hawthorne F.C. and Schindler M. (2008) Understanding the weakly bonded constituents in oxysalt minerals. *Zeitschrift für Kristallographie*, **223**, 41–68.

Higashi T. (2001) *ABSCOR*. Rigaku Corporation, Tokyo.

Kampf A.R., Plášil J., Kasatkin A.V. and Marty J. (2015*a*) Bobcookite, $NaAl(UO_2)_2(SO_4)_4{\cdot}18H_2O$ and wetherillite, $Na_2Mg(UO_2)_2(SO_4)_4{\cdot}18H_2O$, two new uranyl sulfate minerals from the Blue Lizard mine, San Juan County, Utah, USA. *Mineralogical Magazine*, **79**, 695–714.

Kampf A.R., Plášil J., Kasatkin A.V., Marty J. and Čejka J. (2015*b*) Fermiite, $Na_4(UO_2)(SO_4)_3{\cdot}3H_2O$ and oppenheimerite, $Na_2(UO_2)(SO_4)_2{\cdot}3H_2O$, two new uranyl sulfate minerals from the Blue Lizard mine, San Juan County, Utah, USA. *Mineralogical Magazine*, **79**, 1123–1142.

Kampf A.R., Kasatkin A.V., Čejka J. and Marty J. (2015*c*) Plášilite, $Na(UO_2)(SO_4)(OH){\cdot}2H_2O$, a new uranyl sulfate mineral from the Blue Lizard mine, San Juan County, Utah, USA. *Journal of Geosciences*, **60**, 1–10.

Kampf A.R., Plášil J., Kasatkin A.V., Marty J. and Čejka J. (2017*a*) Klaprothite, péligotite and ottohahnite, three new sodium uranyl sulfate minerals with bidentate UO_7–SO_4 linkages from the Blue Lizard mine, San Juan County, Utah, USA. *Mineralogical Magazine* **81**, 753–779.

Kampf A., Plášil J., Kasatkin A., Marty J., Čejka J. and Lapčák L. (2017*b*). Shumwayite, [(UO2)(SO4)(H2O)2]2·H2O, a new uranyl sulfate mineral from Red Canyon, San Juan County, Utah, USA. *Mineralogical Magazine*, **81**, 273–285.

Kampf A., Plášil J., Kasatkin A., Marty J. and Čejka J. (2018*a*) Markeyite, a new calcium uranyl carbonate mineral from the Markey mine, San Juan County, Utah, USA. *Mineralogical Magazine*, **82**, 1089–1100.

Kampf A., Plášil J., Nash B. and Marty J. (2018*b*) Greenlizardite, (NH4)Na(UO2)2(SO4)2(OH)2·4H2O, a new mineral with phosphuranylite-type uranyl sulfate sheets from Red Canyon, San Juan County, Utah, USA. *Mineralogical Magazine*, **82**, 401–411.

Kampf A.R., Plášil J., Nash B.P. and Marty J. (2018*c*) Meitnerite, (NH4)(UO2)(SO4)(OH)·2H2O, a new uranyl-sulfate mineral with a sheet structure. *European Journal of Mineralogy*, **30**, 999–1006.

Kampf A., Olds T., Plášil J., Marty J. and Perry S. (2019) Feynmanite, a new sodium uranyl sulfate mineral from Red Canyon, San Juan County, Utah, USA. *Mineralogical Magazine*, **83**(2), 153–160.

Libowitzky E. (1999) Correlation of O-H stretching frequencies and O–H···O hydrogen bond lengths in minerals. *Monatshefte für Chemie*, **130**, 1047–1059.

Lussier A.J., Lopez A.K. and Burns P.C. (2016) A revised and expanded structure hierarchy of natural and synthetic hexavalent uranium compounds. *The Canadian Mineralogist*, **54**, 177–283.

Mandarino J.A. (1976) The Gladstone-Dale relationship – Part 1: derivation of new constants. *The Canadian Mineralogist*, **14**, 498–502.

Mandarino J.A. (2007) The Gladstone–Dale compatibility of minerals and its use in selecting mineral species for further study. *The Canadian Mineralogist*, **45**, 1307–1324.

Ohwada K. (1976) Infrared spectroscopic studies of some uranyl nitrate complexes. *Journal of Coordination Chemistry*, **6**, 75–80.

Olds T., Sadergaski L., Plášil J., Kampf A., Burns P., Steele I. and Mills O. (2017). Leószilárdite, the first Na,Mg-containing uranyl carbonate from the Markey Mine, San Juan County, Utah, USA. *Mineralogical Magazine*, **81**, 1039–1050.

Plášil J., Buixaderas E., Čejka J., Sejkora J., Jehlička J. and Novák M. (2010) Raman spectroscopic study of the uranyl sulphate mineral zippeite: low wavenumber and U–O stretching regions. *Analytical and Bioanalytical Chemistry*, **397**, 2703–2715.

Plášil J., Kasatkin. A.V., Škoda R., Novák M., Kallistová A., Dušek M., Skála R., Fejfarová K., Čejka J., Meisser N., Goethals H., Machovič V. and Lapčák L. (2013) Leydetite, $Fe(UO_2)(SO_4)_2(H_2O)_{11}$, a new uranyl sulfate mineral from Mas d'Alary, Lodève, France. *Mineralogical Magazine*, **77**, 429–441.

Plášil J., Meisser N. and Čejka J. (2016) The crystal structure of $Na_6[(UO_2)(SO_4)_4](H_2O)_4$: X-ray and Raman spectroscopy study. *The Canadian Mineralogist*, **54**, 5–20.

Pouchou J.-L. and Pichoir F. (1991) Quantitative analysis of homogeneous or stratified microvolumes applying the model "PAP." Pp. 31–75 in: *Electron Probe Quantification* (K.F.J. Heinrich and D.E. Newbury, editors). Plenum Press, New York. Electron Probe Quantitation. Plenum Press, New York.

Quilès F. and Burneau A. (1998) Infrared and Raman spectroscopic study of uranyl complexes: hydroxide and acetate derivatives in aqueous solution. *Vibrational Spectroscopy*, **18**, 61–75.

Serezhkin V.N., Soldatkina M.A. and Efremov V.A. (1981) Crystal structure of $MgUO_2(SO_4)_2{\cdot}11H_2O$. *Zhurnal Strukturnoi Khimii*, **22**, 174–177.

Sheldrick G.M. (2015) Crystal structure refinement with SHELXL. *Acta Crystallographica*, **C71**, 3–8.

Unruh D., Gojdas K., Flores E., Libo A. and Forbes T. (2013) Synthesis and structural characterization of hydrolysis products within the uranyl iminodiacetate and malate systems. *Inorganic Chemistry*, **52**, 10191–10198.

Volkovich V.A., Griffiths T.R., Fray D.J. and Fields M. (1998) Vibrational spectra of alkali metal (Li, Na and K) uranates and consequent assignment of uranate ion site symmetry. *Vibrational Spectroscopy*, **17**, 83–91.

https://doi.org/10.1180/mgm.2018.118 Published online by Cambridge University Press